Photosensitizers

DOI: 10.1002/anie.201204341

Highly Efficient Ultrafast Electron Injection from the Singlet MLCT Excited State of Copper(I) Diimine Complexes to TiO_2 Nanoparticles**

Jier Huang, Onur Buyukcakir, Michael W. Mara, Ali Coskun, Nada M. Dimitrijevic, Gokhan Barin, Oleksandr Kokhan, Andrew B. Stickrath, Romain Ruppert, David M. Tiede, J. Fraser Stoddart, Jean-Pierre Sauvage, and Lin X. Chen**

Photoinduced electron transfer (ET) from transition-metal complexes into semiconductor nanoparticles (NPs) has been studied extensively in recent decades on account of its relevance to photocatalysis, solar fuel generation, and dye-sensitized solar cells (DSSCs).[1] One of the most common DSSC systems utilizes ruthenium polypyridyl complex-sensitized TiO_2 NP electrodes, which provide a relatively high light-to-electron energy conversion efficiency (ca. 11%) in DSSCs.[2] The high cost and low abundance of ruthenium, however, inhibit applications of ruthenium dye-based DSSCs on a large scale. Therefore, dye sensitizers of abundant first-row metal complexes have long been sought. A recent report on porphyrin sensitizer-based DSSCs is one example.[3] Polypyridyl Cu^I complexes are also being considered as a replacement for ruthenium complex sensitizers[4] owing to their striking similarities in absorption spectra and photophysics. However, the efficiencies and stabilities of the devices based on these dyes to date are still inferior in comparison to those of the ruthenium dye-based solar cells. Because many factors can influence the DSSC device efficiency, such as light harvesting, driving force for charge separation and recombination, and excited-state lifetime, an understanding of how these factors can be optimized at molecular and electronic levels is required. In contrast with Ru^{II} polypyridyl complexes, the MLCT states of Cu^I diimine complexes undergo a pseudo Jahn–Teller distortion with significant structural reorganizations and exhibit solvent-dependent lifetimes.[5] More importantly, the intersystem crossing (ISC) rate/yield and thus the ^{1}MLCT state lifetime can be influenced by the coordination geometry of the copper center as well as solvent accessibility.[6,7] Thus, there will be two possible routes to transfer an electron from the photo-excited Cu^I polypyridyl complex to the TiO_2 NPs: 1) from the ^{1}MLCT state with a higher energy and ET driving force but very short excited-state lifetime (that is, ca. 10 ps or shorter); and 2) from the ^{3}MLCT state with a lower energy and ET driving force but much longer excited-state lifetime (a few ns to a few hundred ns). While the excited-state photophysical properties and structural dynamics of several Cu^I complexes have been studied in solution,[6b,7a,8] the electron injection dynamics and its interplay with the sensitizer structure of Cu^I complexes have not been established to date.

Herein, we present highly efficient ultrafast electron injection from the excited state $[Cu^I(dppS)_2]^+$ (dppS = 2,9-diphenyl-1,10-phenanthrolinedisulfonic acid disodium salt) to TiO_2 and correlate the dynamics of charge separation and recombination with the molecular structure (Figure 1) using electron paramagnetic resonance (EPR), optical transient absorption (TA), and X-ray transient absorption (XTA) spectroscopy.[9] The sulfonated phenyl groups at the 2,9 positions of the phenanthroline ligands force the ground state of $[Cu^I(dppS)_2]^+$ to adopt a flattened pseudo-tetrahedral coordination geometry where the spin–orbit coupling is weakened and the copper center is fully shielded from the

[*] Dr. J. Huang, Dr. N. M. Dimitrijevic, Dr. O. Kokhan, Dr. A. B. Stickrath, Dr. D. M. Tiede, Prof. L. X. Chen
Chemical Sciences and Engineering Argonne National Laboratory
Argonne, IL 60439 (USA)
E-mail: lchen@anl.gov

Dr. N. M. Dimitrijevic
Center for Nanoscale Materials, Argonne National Laboratory
Argonne, IL 60439 (USA)

O. Buyukcakir, M. W. Mara, Dr. A. Coskun, G. Barin, Prof. J. F. Stoddart, Prof. L. X. Chen
Department of Chemistry, Northwestern University
2145 Sheridan Road, Evanston, IL 60208 (USA)

Dr. R. Ruppert
Institut de Chimie Université de Strasbourg
67000 Strasbourg (France)

Prof. J.-P. Sauvage
Institut De Science et d'Ingénierie Supramoléculaires
Université de Strasbourg
67000 Strasbourg (France)
E-mail: jpsauvage@unistra.fr

[**] The ultrafast laser and X-ray characterization and analysis are supported by the U.S. Department of Energy, Office of Science, Office of Basic Energy Sciences, Under Contract No. DE-AC02-06CH11357. The synthesis of the complexes is supported as part of the NERC (Non-Equilibrium Research Center), an Energy Frontier Research Center funded by the U.S. Department of Energy, Office of Science, Office of Basic Energy Sciences under the Award Number DE-SC0000989. Use of the Advanced Photon Source at Argonne National Laboratory was supported by the U.S. Department of Energy, Office of Science, Office of Basic Energy Sciences, under Contract No. DE-AC02-06-CH11357. The authors thank Dr. Xiaoyi Zhang, Dr. Kristoffer Haldrup, and Megan Shelby for their assistance in the XTA experiment, and Dr. Xiao-Min Lin for the help in total reflection UV/Vis spectra. O.B. thanks to the Scientific and Technological Research Council of Turkey (TUBITAK) for a fellowship program. MLCT = metal-to-ligand charge transfer.

Supporting information for this article is available on the WWW under http://dx.doi.org/10.1002/anie.201204341.

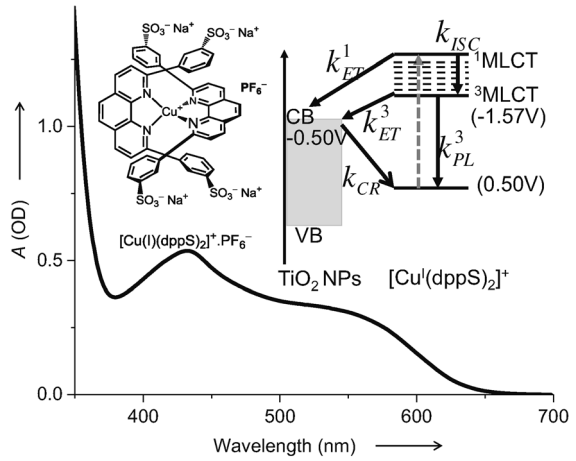

Figure 1. UV/Vis absorption spectrum of $[Cu^{I}(dppS)_2]^+$ in H_2O. Insets: the molecular structure of $[Cu^{I}(dppS)_2]^+$ and the electron-injection and recombination model in the $[Cu^{I}(dppS)_2]^+/TiO_2$ hybrid.

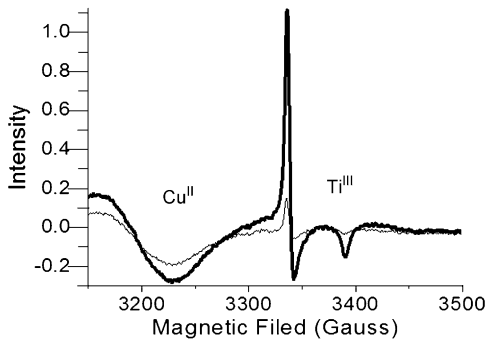

Figure 2. EPR spectra of $[Cu^{I}(dppS)_2]^+/TiO_2$ hybrid under visible light ($\lambda > 440$ nm) illumination (thick line) and after the light was turned off (thin line). The background spectrum collected before illumination has been subtracted from both spectra.

solvent, resulting in an ISC rate constant of about 14 ps (see below). Moreover, the two sulfonated phenyl groups also block solvent access to the Cu center to prevent the formation of an exciplex, which would lower the energy gap between the ^{3}MLCT and the ground states and accelerate the ground-state recovery.[5a,10] Consequently, these structural factors result in longer ^{1,3}MLCT lifetimes and higher emission quantum yields in water. Meanwhile, the sulfonate groups also serve as linkers to TiO_2 NP surfaces through electrostatic or covalent linkages.[11] Details of the experimental setup and sample preparation are described in the Supporting Information. The dppS ligand, as a mixture of *meta*/*meta* (70%) and *meta*/*para* (30%) isomers, was synthesized following a procedure in the literature.[12] The $[Cu^{I}(dppS)_2]^+\cdot PF_6^-$ complex was isolated in 73% yield by mixing the dppS ligand with $[Cu(MeCN)_4]PF_6$ in a MeCN/H_2O solvent at room temperature under a N_2 atmosphere. The oxidation potential of the MLCT state was -1.57 V vs SCE. Compared with the conduction band (CB) edge of TiO_2 NPs (-0.5 V vs SCE),[13] the estimated upper limit of the Gibbs free energy change ΔG_{ET} for ET from the MLCT excited state of $[Cu^{I}(dppS)_2]^+$ to the CB of TiO_2 NPs is -1.07 V.

Steady-state EPR spectra of the $[Cu^{I}(dppS)_2]^+/TiO_2$ hybrid at 5 K were measured to verify the electron injection from the MLCT state of $[Cu^{I}(dppS)_2]^+$ to TiO_2 NPs (see the Supporting Information for details). A Xe lamp with a long pass filter (cut-off wavelength = 440 nm) was used to ensure selective excitation of $[Cu^{I}(dppS)_2]^+$ not TiO_2 NPs. As shown in Figure 2, the EPR spectrum of the $[Cu^{I}(dppS)_2]^+/TiO_2$ hybrid under the light illumination shows distinct features at 3341 and 3388 G, corresponding to $g_\perp = 1.990$ and $g_\parallel = 1.958$, which agree well with the signals for Ti^{III} centers[14] and thus can be assigned to the electrons localized in the TiO_2 NP lattice. The remaining broad features ($g_\perp = 2.078$, $g_\parallel = 2.397$, and $A_\parallel = 120$ G), are characteristic of a Cu^{II} ion in a tetragonally distorted structure,[15] resulting from $[Cu^{II}(dppS)_2]^{2+}$ formed after the electron injection. The intensity of both Ti^{III} and Cu^{II} signals decreased after the lamp was turned off, indicating the recombination of injected electrons in the CB of TiO_2 with the oxidized $[Cu^{II}(dppS)_2]^{2+}$. The characteristic spectral features of the charge separated state, although gradually faded, still remained visible several minutes after the Xe lamp was turned off, suggesting a super-slow charge recombination at 5 K. The results confirm the photoinduced ET from the ^{1,3}MLCT state of $[Cu^{I}(dppS)_2]^+$ to the CB of TiO_2 NPs and the subsequent recombination of the electron in the CB of TiO_2 with $[Cu^{II}(dppS)_2]^{2+}$ in the dark.

Because the electron injection into TiO_2 NPs opens a new decay route for the ^{1,3}MLCT states of $[Cu^{I}(dppS)_2]^+$, the interfacial ET processes can be monitored via the MLCT state absorption signals using TA in the presence and absence of TiO_2 NPs under 415 nm excitation from an ultrafast Ti:sapphire laser system. TA spectra of a reference $[Cu^{I}(dppS)_2]^+/Al_2O_3$ hybrid system, where the electron injection is not feasible, were measured first to account for the MLCT state dynamics of surface-bound $[Cu^{I}(dppS)_2]^+$ (Figure 3a). A broad positive feature was observed in the entire TA spectral range similar with the MLCT state transient absorption of $[Cu^{I}(dppS)_2]^+$ in an aqueous solution (Supporting Information, Figure S4), and it can thus be assigned to the same origin in this reference system. At early delay times (< 50 ps), the broad initial TA at 1 ps delay time grows in the 480–515 nm region and 660–680 nm region, respectively. The growth kinetics in these two regions and the decay dynamics in the 530–650 nm region bordered by the two isosbestic points at 518 and 657 nm correlate well with each other, suggesting that the same dynamic process is associated with the spectral evolution in the three regions. The kinetic traces in the 480–515 and 660–680 nm regions (Figure 3c), fit by single-exponential rise and decay functions, both show a fast rise (13.7 ps) and a slow decay ($\gg 3$ ns) time constants, which correlate well with the two decay time constants of $t_1 = 13.7$ ps (25%) and $t_2 \gg 3$ ns (75%) in the 530–650 nm region fit by a bi-exponential decay function. The shorter time constant $t_1 = 13.7$ ps is consistent with the ISC time constant previously observed after the excited-state flattening owing to the Jahn–Teller distortion as the Cu center changes from $3d^{10}$ to $3d^9$.[6,8e] The long decay time constant of $\gg 3$ ns is attributed to the ^{3}MLCT state decay, which is too long to be determined accurately in the femtosecond TA time window. In the delay time window of about 50 ps to 3 ns, slight deviations of the

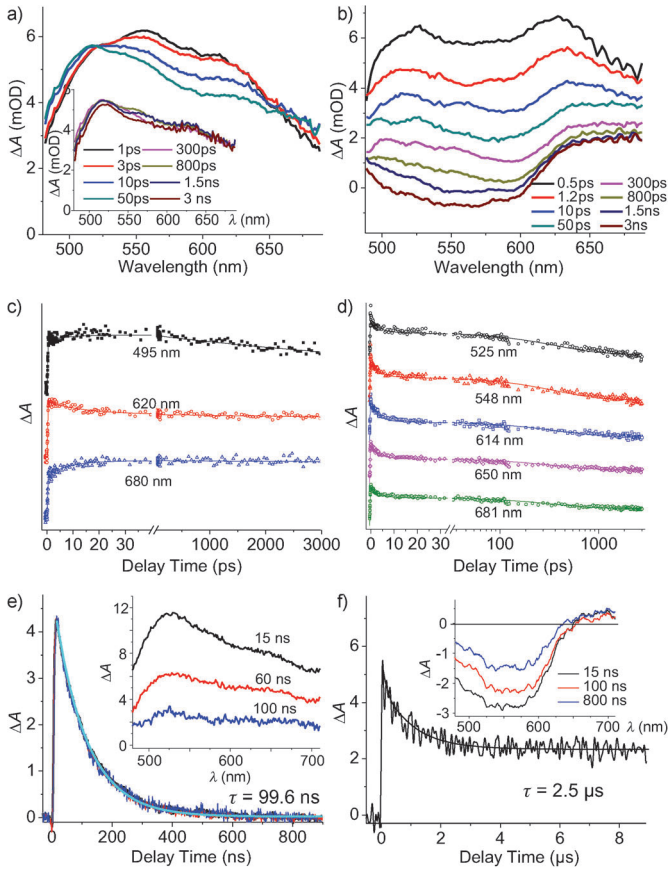

Figure 3. a,b) Femtosecond TA spectra of a) $[Cu^{I}(dppS)_2]^+/Al_2O_3$ and b) $[Cu^{I}(dppS)_2]^+/TiO_2$ hybrids under 415 nm excitation. c,d) Transient kinetics curves at different probe wavelengths as labeled for c) $[Cu^{I}(dppS)_2]^+/Al_2O_3$ and d) $[Cu^{I}(dppS)_2]^+/TiO_2$ hybrids. The curves are displayed with the *y* axis offset for clarity. The symbols are experimental data and the solid curves are the fits. e,f) Nanosecond absorption kinetics of e) $[Cu^{I}(dppS)_2]^+/Al_2O_3$ at 500 nm (black), 570 nm (red), and 700 nm (blue) with the fit (cyan) to all the curves, and f) of $[Cu^{I}(dppS)_2]^+/TiO_2$ at 700 nm. Inset: nanosecond absorption spectra of e) $[Cu^{I}(dppS)_2]^+/Al_2O_3$ and f) $[Cu^{I}(dppS)_2]^+/TiO_2$. The absolute amplitudes of the kinetic traces in (e) were scaled for comparison purposes.

kinetic traces in the 480–515 nm region and in the 660–680 nm region was observed; the origin of this difference is unclear. To accurately measure the long decay time constants for the ^{3}MLCT state, we collected the kinetics traces in a time window of several hundred nanoseconds using a nanosecond photolysis apparatus at three different probe wavelengths, namely 500 nm, 570 nm and 700 nm, and observed consistency among the three kinetic curves (Figure 3e). Fitting the individual kinetics at the three probe wavelengths by exponential decay functions yields the same decay time constant of 99.6 ns, which agrees with the result from previous studies on $[Cu^{I}(dppS)_2]^+$ in solution.[16]

Compared to the reference TA spectra of $[Cu^{I}(dppS)_2]^+/Al_2O_3$ (Figure 3a), the TA spectra of $[Cu^{I}(dppS)_2]^+/TiO_2$ measured under the same conditions (Figure 3b) are drastically different in spectral shape and show much faster decay kinetics at early times. As the delay time *t* increases, a valley-like feature centered at 570 nm becomes more pronounced and then evolves into a broad bleach band centered at 550 nm at $t > 1.5$ ns. This feature, assigned as the ground-state bleach, is sustained in the nanosecond TA spectra (inset of Figure 3f) and becomes more clear after the MLCT state absorption signal decays substantially owing to the electron injection. All of these facts suggest ET from the excited $[Cu^{I}(dppS)_2]^+$ to TiO_2 NPs, which is consistent with the EPR measurement discussed earlier.

In principle, the ET and CR (charge recombination) rates can be measured by the TA signals of $[Cu^{II}(dppS)_2]^{2+}$, but such measurements have been proven to be difficult because of the low extinction coefficient of $[Cu^{II}(dppS)_2]^{2+}$ compared to the ground state $[Cu^{I}(dppS)_2]^+$ and its spectral overlap with the ground-state bleach and excited-state absorption. To circumvent this difficulty, the ET rate in this study was extracted quantitatively by global fitting the kinetics traces at different probe wavelengths. At probe wavelength λ, the TA signal ($S(\lambda, t)$) is given by the sum of the TA signals of the MLCT excited state absorption, the ground-state bleach, and the ET generated $[Cu^{II}(dppS)_2]^{2+}$ state absorption:

$$\begin{aligned} S(\lambda,t) =& \varepsilon^1(\lambda)N^1(t) + \varepsilon^3(\lambda)N^3(t) \\ & -\varepsilon^0(\lambda)[N^1(t) + N^3(t) + N^+(t)] + \varepsilon^+(\lambda)N^+(t) \end{aligned} \quad (1)$$

where ($\varepsilon^1(\lambda)$, $N^1(t)$), ($\varepsilon^3(\lambda)$, $N^3(t)$,), and ($\varepsilon^+(\lambda)$, $N^+(t)$) are the extinction coefficients and concentrations of ^{1}MLCT, ^{3}MLCT, and the ET generated $[Cu^{II}(dppS)_2]^{2+}$ states, respectively. Assuming that the ET rate is much faster than the ^{3}MLCT state intrinsic decay and the charge recombination rate, we can use the following equations to express the concentrations of the above species:

$$\begin{aligned} N^1(t) &= N_0 e^{-(k^1_{ET}+k_{ISC})t} \\ N^3(t) &= N_0 \frac{k_{ISC}}{k^3_{ET} - k_{ISC} - k^1_{ET}} [e^{-(k^1_{ET}+k_{ISC})t} - e^{-k^3_{ET}t}] \\ N^+(t) &= N_0 [-\frac{k^1_{ET}}{k^1_{ET} + k_{ISC}} e^{-(k^1_{ET}+k_{ISC})t} - \frac{k_{ISC}}{k^1_{ET} + k_{ISC}} e^{-k^3_{ET}t}] \end{aligned} \quad (2)$$

where k^1_{ET} and k^3_{ET} are rate constants for ET from singlet MLCT and triplet MLCT states, respectively. k_{ISC} is the intrinsic ISC rate constant determined by fitting the TA decay of the $[Cu^{I}(dppS)_2]^+$ MLCT excited state in the reference $[Cu^{I}(dppS)_2]^+/Al_2O_3$ hybrid. N^0 is the total excited state concentration at time 0. If multiple binding configurations exist, such as $[Cu^{I}(dppS)_2]^+$ binding with a single or double sulfonate linker(s), multiple sets of Equation (2) can appear in the TA signal fitting. According to this model, we can satisfactorily fit the kinetics at 525, 548, 614, 650, and 681 nm simultaneously by using the same rate constants while varying the extinction coefficients, as shown in Figure 3d. Restriction is given by the known extinction coefficients of ground-state and oxidized-state absorption at different wavelengths. The time constants with the best fit (Supporting Information, Table S1) for ET process are 0.4 ps and 12 ps for ET from ^{1}MLCT state, and 1000 ps for ET from ^{3}MLCT. These results suggest an efficient ultrafast electron injection from ^{1}MLCT state to the TiO_2 NPs.

The CR dynamics of the $[Cu^{I}(dppS)_2]^+/TiO_2$ hybrid was also measured by the nanosecond TA setup. In the absence of the ET to TiO_2 NPs, the TA spectra of $[Cu^{I}(dppS)_2]^+/Al_2O_3$

(Figure 3e, inset) are mostly due to the ^{3}MLCT state absorption in the nanosecond regime. In contrast, the TA spectra of $[Cu^I(dppS)_2]^+/TiO_2$ (inset of Figure 3f) show a broad ground-state bleach feature in the 480–620 nm region and an absorption at >620 nm, which are mainly due to the absorption features from both $[Cu^{II}(dppS)_2]^{2+}$ and CB electrons of the TiO_2 NPs as seen in the ground state $[Cu^{II}(dppS)_2]^{2+}$ (Supporting Information, Figure S5) and other DSSC mimics, respectively.[17] Therefore, these absorption features can be used to monitor the CR process; that is, back ET from CB of the TiO_2 NPs to $[Cu^{II}(dppS)_2]^{2+}$, which will cause the decay of these signals as shown in Figure 3f. The decay kinetics can be adequately fit by a three-exponential function with time constants of 270 ns (44%), 1.2 μs (19%), and $\gg 9$ μs (37%), corresponding to kinetics of the CR process that are several orders of magnitude slower than the ET process, suggesting efficient charge separation processes in this hybrid system.

The ET process in $[Cu^I(dppS)_2]^+/TiO_2$ can also be monitored by probing the oxidation state of the Cu center using XTA at the Cu K-edge with and without the laser excitation (for details, see the Supporting Information). Figure 4 shows XANES (X-ray absorption near-edge structure) spectra of $[Cu^I(dppS)_2]^+/TiO_2$ with the ground state and laser initiated state, as well as the oxidized state after electron injection to TiO_2 NPs. The oxidized-state spectrum was

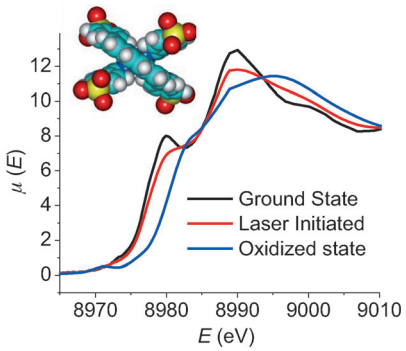

Figure 4. The XANES spectra of $[Cu^I(dppS)_2]^+$ in the $[Cu^I(dppS)_2]^+/TiO_2$ hybrid at the Cu K edge. The laser-initiated scan was collected at a laser time delay of 9 ns.

obtained by subtracting the contribution of about 75% of the remaining ground state from the laser initiated spectrum. The laser initiated spectrum was taken at 9 ns delay time well after the electron injection, when only a negligible fraction ($\ll 0.1$%) of the MLCT state population remained according to the TA results. Therefore, the contribution of excited state to the XANES spectral changes caused by the laser pump pulse can be excluded. Three distinct changes are observed in the laser-initiated XANES spectrum compared to the ground state spectrum: 1) a reduced shoulder feature at 8.979 keV; 2) a reduced intensity at 8.987 keV; and 3) an increase of the intensity at 8.998 keV. These features are seen when $[Cu^{II}(dppS)_2]^{2+}$ is generated electrochemically or photochemically[6b,7a,8b,d] and hence further confirm the ET to the TiO_2 NPs, consistent with the EPR and TA results. Compared to previously studied $[Cu^I(dmp)_2]^+$,[8b,d] the shoulder feature in the XANES spectra of $[Cu^I(dppS)_2]^+$ at 8.979 keV, assigned as the 1s to $4p_z$ transition, has a higher intensity owing to a flattened tetrahedral coordination geometry for the copper center in the ground state (Figure 4 inset),[18] where the spin-orbit coupling is significantly weakened and thus results in a much slower ISC process with a time constant of 13.7 ps, which is more than a factor of 200 slower than the ISC process in the well-studied ruthenium based dye sensitizers.[19,20] Therefore, we have demonstrated that the coordination symmetry of $[Cu^I(dppS)_2]^+$ effectively modulates its excited-state properties, facilitating a direct electron injection pathway from the ^{1}MLCT state of $[Cu^I(dppS)_2]^+$ to TiO_2 NPs before its ISC generates the low-energy ^{3}MLCT state. Without the steric hindrance of the two phenyl groups in the 2 and 9 positions of phenanthroline ligands, the two dppS ligands in the complex will be nearly orthogonal to each other, resulting in a stronger spin–orbit coupling and thus a much faster ISC process may take place.[7a]

In summary, a highly efficient and ultrafast interfacial electron injection from the ^{1}MLCT state of surface bound $[Cu^I(dppS)_2]^+$ to TiO_2 NPs has been observed in EPR, TA, and XTA studies, with the charge separation and recombination dynamics correlated with the ground- and excited-state structures. These studies confirmed the formation of $[Cu^{II}(dppS)_2]^{2+}$, resulting from an efficient charge-transfer process in $[Cu^I(dppS)_2]^+/TiO_2$ where electrons are injected into TiO_2 NPs. The flattened tetrahedral geometry of the ground state $[Cu^I(dppS)_2]^+$ in the hybrid system as detected by the XTA effectively prolongs the ISC time to enable ET from the ^{1}MLCT state. Further studies in tuning the HOMO–LUMO levels of these complexes by structural constraints will be conducted in the future. This research not only demonstrates the structural control necessary for effective ET processes, but also shows the potential of using low-cost copper complexes for the dye-sensitized solar cells in the future.

Received: June 4, 2012
Revised: October 4, 2012
Published online: November 8, 2012

Keywords: charge transfer · complexes · copper · nanoparticles · structural dynamics

[1] a) A. Hagfeldt, M. Grätzel, *Chem. Rev.* **1995**, *95*, 49; b) J. E. Moser, P. Bonnôte, M. Gratzel, *Coord. Chem. Rev.* **1998**, *171*, 245; c) N. Serpone, *Res. Chem. Intermed.* **1994**, *20*, 953; d) P. V. Kamat, *Chem. Rev.* **1993**, *93*, 267; e) R. J. D. Miller, G. L. McLendon, A. J. Nozik, W. Schmickler, F. Willig, *Surface electron transfer processes*, VCH publishers, New York, **1995**.

[2] a) K. Sayama, H. Sugihara, H. Arakawa, *Chem. Mater.* **1998**, *10*, 3825; b) J. B. Asbury, E. Hao, Y. Q. Wang, H. N. Ghosh, T. Q. Lian, *J. Phys. Chem. B* **2001**, *105*, 4545; c) Y. Tachibana, S. A. Haque, I. P. Mercer, J. E. Moser, D. R. Klug, J. R. Durrant, *J. Phys. Chem. B* **2001**, *105*, 7424; d) R. J. Ellingson, J. B. Asbury, S. Ferrere, H. N. Ghosh, J. R. Sprague, T. Q. Lian, A. J. Nozik, *J. Phys. Chem. B* **1998**, *102*, 6455; e) D. Kuciauskas, J. E. Monat, R. Villahermosa, H. B. Gray, N. S. Lewis, J. K. McCusker, *J. Phys. Chem. B* **2002**, *106*, 9347; f) T. A. Heimer, E. J. Heilweil, C. A. Bignozzi, G. J. Meyer, *J. Phys. Chem. A* **2000**, *104*, 4256; g) J.

Kallioinen, G. Benkö, V. Sundström, J. E. I. Korppi-Tommola, A. P. Yartsev, *J. Phys. Chem. B* **2002**, *106*, 4396.
[3] A. Yella, H. W. Lee, H. N. Tsao, C. Y. Yi, A. K. Chandiran, M. K. Nazeeruddin, E. W. G. Diau, C. Y. Yeh, S. M. Zakeeruddin, M. Grätzel, *Science* **2011**, *334*, 629.
[4] a) N. Alonso-Vante, J. F. Nierengarten, J. P. Sauvage, *J. Chem. Soc. Dalton* **1994**, 1649; b) S. K. Sakaki, T. Kuroki, T. Hamada, *J. Chem. Soc. Dalton Trans.* **2002**, 840; c) T. Bessho, E. C. Constable, M. Grätzel, A. H. Redondo, C. E. Housecroft, W. Kylberg, M. K. Nazeeruddin, M. Neuburger, S. Schaffner, *Chem. Commun.* **2008**, 3717.
[5] a) D. R. McMillin, J. R. Kirchhoff, K. V. Goodwin, *Coord. Chem. Rev.* **1985**, *64*, 83; b) D. V. Scaltrito, D. W. Thompson, J. A. O'Callaghan, G. J. Meyer, *Coord. Chem. Rev.* **2000**, *208*, 243; c) C. T. Cunningham, K. L. H. Cunningham, J. F. Michalec, D. R. McMillin, *Inorg. Chem.* **1999**, *38*, 4388.
[6] a) Z. A. Siddique, Y. Yamamoto, T. Ohno, K. Nozaki, *Inorg. Chem.* **2003**, *42*, 6366; b) G. B. Shaw, C. D. Grant, H. Shirota, E. W. Castner, G. J. Meyer, L. X. Chen, *J. Am. Chem. Soc.* **2007**, *129*, 2147.
[7] a) J. V. Lockard, S. Kabehie, J. I. Zink, G. Smolentsev, A. Soldatov, L. X. Chen, *J. Phys. Chem. B* **2010**, *114*, 14521; b) N. A. Gothard, M. W. Mara, J. Szarko, J. V. Lockard, S. T. Nguyen, L. X. Chen, *Abstr. Pap. Am. Chem. Soc.* **2011**, 241.
[8] a) M. Ruthkosky, C. A. Kelly, F. N. Castellano, G. J. Meyer, *Coord. Chem. Rev.* **1998**, *171*, 309; b) L. X. Chen, G. Jennings, T. Liu, D. J. Gosztola, J. P. Hessler, D. V. Scaltrito, G. J. Meyer, *J. Am. Chem. Soc.* **2002**, *124*, 10861; c) G. Smolentsev, A. V. Soldatov, L. X. Chen, *J. Phys. Chem. A* **2008**, *112*, 5363; d) L. X. Chen, G. B. Shaw, I. Novozhilova, T. Liu, G. Jennings, K. Attenkofer, G. J. Meyer, P. Coppens, *J. Am. Chem. Soc.* **2003**, *125*, 7022; e) M. Iwamura, S. Takeuchi, T. Tahara, *J. Am. Chem. Soc.* **2007**, *129*, 5248; f) M. Iwamura, H. Watanabe, K. Ishii, S. Takeuchi, T. Tahara, *J. Am. Chem. Soc.* **2011**, *133*, 7728.
[9] a) L. X. Chen, *Angew. Chem.* **2004**, *116*, 2946; *Angew. Chem. Int. Ed.* **2004**, *43*, 2886; b) L. X. Chen, *Annu. Rev. Phys. Chem.* **2005**, *56*, 221.
[10] E. M. Kober, J. V. Caspar, R. S. Lumpkin, T. J. Meyer, *J. Phys. Chem.* **1986**, *90*, 3722.
[11] a) C. Bauer, P. Jacques, A. Kalt, *Chem. Phys. Lett.* **1999**, *307*, 397; b) M. Stylidi, D. I. Kondarides, X. E. Verykios, *Appl. Catal. B* **2003**, *40*, 271.
[12] J. P. Collin, R. Ruppert, J. P. Sauvage, *Nouv. J. Chim.* **1985**, *9*, 395.
[13] E. Palomares, J. N. Clifford, S. A. Haque, T. Lutz, J. R. Durrant, *J. Am. Chem. Soc.* **2003**, *125*, 475.
[14] D. C. Hurum, A. G. Agrios, K. A. Gray, T. Rajh, M. C. Thurnauer, *J. Phys. Chem. B* **2003**, *107*, 4545.
[15] a) M. Geoffroy, M. Wermeille, C. O. Buchecker, J. P. Sauvage, G. Bernardinelli, *Inorg. Chim. Acta* **1990**, *167*, 157; b) F. Baumann, A. Livoreil, W. Kaim, J. P. Sauvage, *Chem. Commun.* **1997**, 35.
[16] C. O. Dietrich-Buchecker, P. A. Marnot, J. P. Sauvage, J. R. Kirchhoff, D. R. Mcmillin, *J. Chem. Soc. Chem. Commun.* **1983**, 513.
[17] A. Safrany, R. M. Gao, J. Rabani, *J. Phys. Chem. B* **2000**, *104*, 5848.
[18] L.-S. Kau, D. J. Spira-Solomon, J. E. Penner-Hahn, K. O. Hodgson, E. I. Solomon, *J. Am. Chem. Soc.* **1987**, *109*, 6433.
[19] A. C. Bhasikuttan, M. Suzuki, S. Nakashima, T. Okada, *J. Am. Chem. Soc.* **2002**, *124*, 8398.
[20] a) O. Bräm, F. Messina, A. M. El-Zohry, A. Cannizzo, M. Chergui, *Chem. Phys.* **2012**, *393*, 51; b) O. Bräm, A. Cannizzo, M. Chergui, *Phys. Chem. Chem. Phys.* **2012**, *14*, 7934.

